Mechanics of Advanced Materials and Structures

ISSN: (Print) (Online) Journal homepage: https://www.tandfonline.com/loi/umcm20

A study of crack propagation during blasting under high in-situ stress conditions based on an improved CDEM method

Chenxi Ding, Xintong Liang, Renshu Yang, Zong-Xian Zhang, Xiao Guo, Chun Feng, Xinguang Zhu & Quanmin Xie

To cite this article: Chenxi Ding, Xintong Liang, Renshu Yang, Zong-Xian Zhang, Xiao Guo, Chun Feng, Xinguang Zhu & Quanmin Xie (2023): A study of crack propagation during blasting under high in-situ stress conditions based on an improved CDEM method, Mechanics of Advanced Materials and Structures, DOI: 10.1080/15376494.2023.2208112

To link to this article: https://doi.org/10.1080/15376494.2023.2208112

Published online: 09 May 2023.

MECHANICS OF ADVANCED MATERIALS AND STRUCTURES
https://doi.org/10.1080/15376494.2023.2208112

Taylor & Francis
Taylor & Francis Group

ORIGINAL ARTICLE

A study of crack propagation during blasting under high in-situ stress conditions based on an improved CDEM method

Chenxi Ding[a,b,c], Xintong Liang[a,b], Renshu Yang[a,b], Zong-Xian Zhang[d], Xiao Guo[e], Chun Feng[f], Xinguang Zhu[f], and Quanmin Xie[c]

[a]School of Civil and Resource Engineering, University of Science and Technology Beijing, Beijing, China; [b]Key Laboratory of Ministry of Education for High-Efficient Mining and Safety of Metal Mines, University of Science and Technology Beijing, Beijing, China; [c]Hubei Key Laboratory of Blasting Engineering, Jianghan University, Wuhan, China; [d]Oulu Mining School, University of Oulu, Oulu, Finland; [e]School of Mathematics and Physics, University of Science and Technology Beijing, Beijing, China; [f]Key Laboratory for Mechanics in Fluid Solid Coupling Systems, Institute of Mechanics, Chinese Academy of Sciences, Beijing, China

ABSTRACT

Considering the energy consumption of the crushed zone caused by blasting, the energy dissipation characteristics were investigated through theoretical calculation and a plug-in for calculation of energy reduction was made. As a result, an improved CDEM method suitable for studying blast-induced crack propagation was proposed. The improved CDEM method was then used to numerically simulate the blast-induced crack propagation under three different in-situ stress conditions: uniaxial in-situ stress, biaxial equal in-situ stresses and biaxial unequal in-situ stresses. It was found that the in-situ stress conditions had significant effects on the distribution of the blast-induced cracks, the evolution of blast-induced stresses and the propagation of the blast-induced cracks. At the uniaxial in-situ stress condition, the vertical in-situ stress reduced the tip stresses of the horizontal crack and inhibited the propagation of the horizontal crack. At the biaxial equal in-situ stress condition, the peak radial stresses and circumferential stresses of the gauging points decreased gradually with the increase of in-situ stresses. In particular, the circumferential stresses of the gauging points gradually changed from tension to compression with an increasing in-situ stress. At the biaxial unequal in-situ stress condition, there were different inhibitions on crack propagation in the horizontal direction and the vertical one.

ARTICLE HISTORY
Received 29 November 2022
Accepted 25 April 2023

KEYWORDS
Crushed zone; energy dissipation; in-situ stress; crack propagation; stress evolution

1. Introduction

With an increasing population and GDP per capita, the global production and consumption of various minerals have increased for over one century [1]. The stock of mineral resources in the shallow earth has been difficult to meet the needs of industrial production, and exploration into the deep earth is an inevitable development trend. In the deep environment, resource exploitation faces high in-situ stresses with the prominent nonlinear characteristics of rock mass and mining difficulty increases dramatically [2]. The high in-situ stresses mentioned above are a big challenge for rock blasting in deep mines or other deep rock projects. The propagation of cracks under explosion load has been extensively studied [3–5].

In deep mining, the in-situ stresses such as vertical stress increase significantly with the increase of mining depth [6]. The results of in-situ stress researches show that when the depth reaches 500 m, the in-situ stress exceeds 10 MPa. When the depth gradually increases, the in-situ stress increases linearly [7, 8]. Therefore, in the deep rock blasting, rock fracture is due to a combined action of in-situ stresses and blast-induced stresses, so the influence of the in-situ stresses on blast results cannot be ignored [9]. Previous studies have shown that in-situ stresses have a significant effect on the stress state around the borehole [10], the propagation characteristics of blasting stress waves [11] and blast-induced cracks [12]. Because the blast-induced crack propagation at high in-situ stress conditions is closely related to the design of blasting parameters, it has received more extensive attention.

Kutter and Fairhurst [13] investigated the effect of in-situ stress field on the distribution of blast-induced cracks through model experiments. They showed that the in-situ stress field promoted the propagation of blast-induced cracks along the direction of the maximum principal stress and inhibited the propagation of blast-induced cracks perpendicular to the direction of the maximum principal stress. In the following decades, the experimental results of Kutter and Fairhurst were verified by other researchers by means of model experiments [14, 15]. Although the model experiments can reflect the influence of in-situ stress on the propagation of blast-induced cracks more realistically, due to the complexity of experimental loading and the limitations of testing methods, it is difficult to collect the data of

CONTACT Xintong Liang Arya1113@163.com School of Civil and Resource Engineering, University of Science and Technology Beijing, Beijing 100083, China.

in-situ stress effect on the propagation of blast-induced cracks. Therefore, numerical simulation has become a necessary approach to study the propagation of blast-induced cracks in high in-situ stress rock mass in recent years. Zhang et al. [16] simplified rock blasting with a columnar charge in an infinite rock mass into a plane strain problem. Based on the bilinear kinematic hardening yield theory, they studied the effect of the in-situ stress field on the crack propagation using finite element method (FEM). Their simulation results showed that the area of circular fracture zone decreased nonlinearly with the increase of in-situ stresses at the biaxial equal in-situ stress condition. Using LS-DYNA software, Xie et al. [17] used the Riedel-Hiermaier-Thoma (RHT) model to study the crack propagation and damage distribution of cut blasting at high in-situ stress conditions with different lateral pressure coefficients. Their results provided a reference for the parameter design of deep rock cut blasting. Wei et al. [18] used the Rock Failure Process Analysis (RFPA) software to conduct a numerical simulation of crack propagation of slit charge blasting at high in-situ stress conditions. Their study indicated that when the maximum principal stress direction of the in-situ stress field was perpendicular to the slit direction, it was not conducive to the propagation of the directional crack. While when the direction of the maximum principal stress was parallel to the slit direction, it was favorable for the propagation of the directional crack. Their results provided a guide line for optimization of blasting parameters in deep rock excavation. Han et al. [19–22] implemented combined finite-discrete element method (FDEM) parallelized on the basis of GPGPU to model the rock fracture and fragmentation process and study the damage evolution during controlled contour blasting in the bench of a deep-buried tunnel, and applied the self-developed combined finite-discrete element method software to model the rock fracture process induced by a single-hole destress blasting based on a practical blast in a deep gold mine with high in-situ stresses. Besides, the FDEM numerical modeling vividly simulates the fracture initiation and propagation, as well as the fragment expulsion, ejection and flyout resulting in the rockburst process that could be difficult to capture on the site or *via* the conventional continuum modellings. An et al. [23] implemented hybrid finite-discrete element method (FEM-DEM) to simulate rock fracture and resultant fragment muck-piling in various blasting scenarios. Zheng et al. [24] studied the blasting damage of single free boundary media and evaluated the damage based on fractal theory.

The above description indicates that the numerical simulation of blast-induced crack propagation at high-in-situ stress conditions has been mainly carried out using the finite element method. For the algorithm principle of numerical simulation, the finite element method cannot be used to simulate blast-induced crack propagation. As a result, on the one hand, important dynamic parameters such as the stresses of a crack tip at high in-situ stress conditions cannot be obtained in the numerical simulation; on the other hand, the reliability of the existing conclusions obtained from the finite element method requires validation. As above, this study adopts a method combining finite element and discrete element to carry out the numerical simulation of crack propagation at high in-situ stress conditions. This study aims to simulate the propagation of blast-induced cracks more realistically and to investigate the effect of different in-situ stress states on the blast-induced crack distribution.

2. Improved CDEM method

2.1. Introduction of CDEM

The Continuum Discontinuum Element Method (CDEM) [25, 26], based on the Lagrangian's equation, realizes the coupling of finite element and discrete element and simulates the internal and boundary fracture of a block. The method can simulate the progressive failure process of a material (As shown in Figure 1) using a block to represent a continuous property and using an interface to represent a discontinuous property. The GDEM software used in this study is based on the CDEM method, which simulates the entire dynamic process of the block from continuous deformation to crack propagation. Therefore, GDEM can simulate the physical process of crack propagation more realistically.

2.2. Improved CDEM method

Rock fragmentation by blasting is a complex process. The rock fragmentation depends not only on the energy input to the system, but also on the energy distribution or effective energy used in rock fragmentation [28, 29]. The region of a blast can be divided or partitioned into crushed zone, fracture zone, and elastic vibration zone that are located consecutively from the vicinity of the borehole to distant locations [30]. Under the strong impact of the detonation wave, a small area around the borehole is crushed to form a crushed zone [31]. Although the scope of the crushed zone is small, relevant studies have shown that 50% of the energy generated by conventional explosives is used to form the crushed zone. As a result, only 20–30% of the blasting energy is effectively used to break the rock [32–34]. The CDEM method mainly controls the crack propagation in a structure through fracture energy. This method has been successfully applied in the study of bench blasting and cut blasting. The CDEM method can simulate the formation process of the fracture zone. However, due to the complexity of blasting process, there is no numerical software that can simulate the formation process of the crushed zone. In the numerical simulation of blasting by CDEM method, the fracture zone is directly formed around the borehole without considering the formation of the crushed zone. Although the scope of the crushed zone which is small can be ignored, the blasting energy consumed by the crushed zone is nonnegligible.

At present, the CDEM method does not consider the consumption of blasting energy in the crushed zone, resulting in too much energy being used to form the fracture zone, and the algorithm design is not reasonable enough. Therefore, it is necessary to obtain the energy consumption of the crushed zone and realize the reduction of the energy input to the fracture zone, so as to simulate the propagation

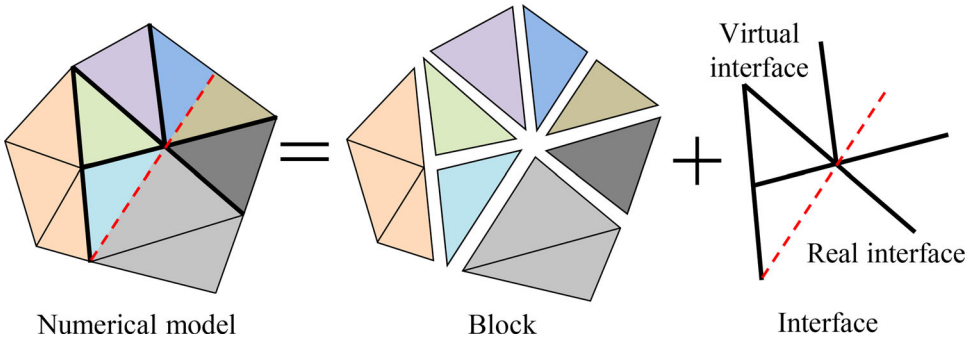

Figure 1. Basic components of CDEM numerical models [27].

behavior of blast-induced cracks more realistically. In the calculation, it is considered that the rock in the crushed zone is completely destroyed by the strong compression and shear load, and a pulverized cavity area is formed. The rock in this region can be regarded as an isotropic, incompressible and non-cohesive bulk medium, but still has cohesion between the broken particles. The model is simplified as an infinitely long cylindrical cavity in the rock medium. The cavity is subjected to a blasting stress uniformly distributed along the axial direction. The blasting gas is assumed to propagate adiabatically. The volume of the gas in the fracture is negligible.

According to the Mohr-Coulomb criterion of rock failure and the Jones-Miller adiabatic equation, the radius r_c of the crushed zone is given by [34]:

$$r_c = r_b\left(\frac{P_b}{\sigma_s}K^{\frac{\sin\theta}{1+\sin\theta}}\right)^{\frac{1}{2\gamma_1}}K^{-0.5} \tag{1}$$

where r_b is the radius of the borehole; P_b is the original pressure of the borehole after the detonation (Chapman-Jouguet pressure in the case of coupling charge); θ is the internal friction angle; γ_1 is the adiabatic index in the initial stage (γ_1 =3.0); K is a coefficient.

The dynamic compressive strength σ_s of rock is [35]:

$$\sigma_s = \sigma_c\left(\frac{\rho_m {c_p}^2}{\sigma_c}\right)^{1/4} \tag{2}$$

where σ_c is compressive strength; ρ_m is the density of the rock; c_p is the velocity of longitudinal wave.

On this basis, according to the energy conservation law, the energy consumption in the crushed zone includes fracture surface energy E_F, deformation energy E_P, kinetic energy of rock movement and other forms of energy [27]. Due to the clamping effect of the rock around the borehole, the fine particles in the crushed zone will not splash, and its kinetic energy will eventually be converted into the surface energy and deformation energy of rock crushing. Moreover, other forms of energy account for a small proportion which can be ignored in the calculation. The energy consumption of the crushed zone is given by:

$$E = E_F + E_P \tag{3}$$

where E is the energy consumption of crushed zone; E_F is the energy required for per additional surface; E_P is the energy required for plastic deformation [36].

Assuming that the fine particles in the crushed zone are infinitely small equal diameter circles, then the total surface area S_1 of the fine particles in the crushed zone of every cross section after blasting is given by:

$$S_1 = \frac{2\pi({r_c}^2 - {r_b}^2)}{x} \tag{4}$$

where x is the radius of the fine particles in crushed zone.

The surface area of the original structural S_2 of the crushed zone before blasting:

$$S_2 = 2\pi(r_c + r_b) \tag{5}$$

The energy E_F required for per additional surface and the energy E_P required for plastic deformation are respectively calculated by:

$$E_F = E_F^{\mathrm{II}} - {E_F}^{\mathrm{I}} \tag{6}$$

that is

$$E_F = G_F\left[\frac{2\pi({r_c}^2 - {r_b}^2)}{x} - 2\pi(r_c + r_b)\right] \tag{7}$$

$$E_P = \pi{\sigma_s}^2({r_c}^2 - {r_b}^2)\frac{3(1-2\upsilon)}{2E} \tag{8}$$

Where E_F^{II} is the fracture energy per unit surface area in the crushed zone after blasting; E_F^{I} is the surface energy of the crushed zone before blasting; G_F is the rock surface energy per unit area; υ is Poisson's ratio; E is elastic modulus.

The CDEM method mainly uses the Landau-Stanyukovich equation (γ equation) to calculate the pressure of the blasting gas. Firstly, the transient pressure is calculated from the current volume of the explosive unit. This pressure acts on the rock unit at the corresponding position. Then the rock unit will produce corresponding displacement due to the pressure, which will affect the volume of the explosive unit. Such cyclic calculation realizes the real-time simulation of crack propagation. The calculation process of the crack propagation model in the CDEM method can be summarized as Figure 2.

Since the whole simulation calculation without full consideration of the huge energy consumption of the crushed zone at the moment of detonation. After the theoretical radius and energy consumption of the crushed zone are obtained through the calculations above, the CDEM crushed

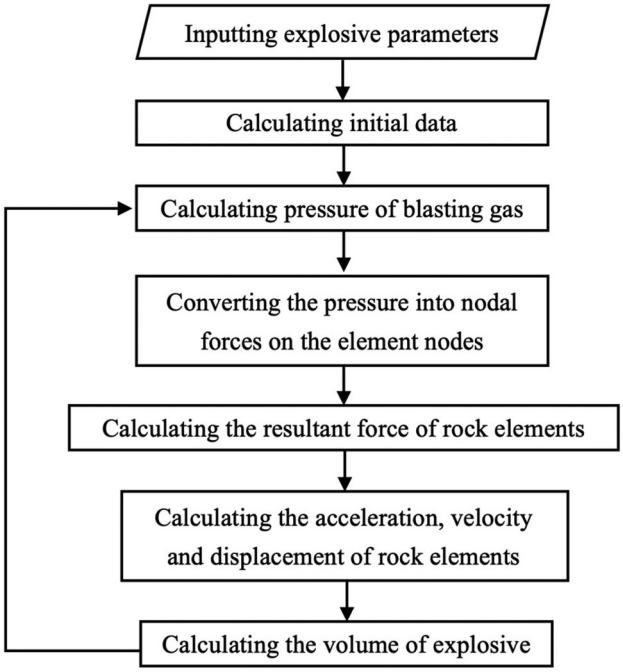

Figure 2. The calculation process of the crack propagation in CDEM.

zone energy consumption reduction plug-in is made. For taking full advantage of the built model for subsequent analyzing and calculating, the parameters required for the calculation of energy consumption are first summarized. Then the interface function "blkdyn.GetElemValue" to call the parameter values in the model and the JavaScript language to call the mathematical functions are used to finish the algorithm plug-in of energy consumption, thereby the energy consumption calculation and energy reduction of the crushed zone can be completed. The plug-in is set to run after the input of the explosive parameters, so that the software can automatically complete the energy reduction of the crushed zone. The improved CDEM method takes into account the energy loss in the crushed zone and reduces the energy by plug-in, which makes the numerical simulation results closer to the physical process of blast-induced crack propagation and provides a better numerical simulation software for the subsequent research.

2.3. Case verification

In order to verify the applicability of the improved CDEM method considering the energy consumption of the crushed zone, numerical simulation of single-borehole blasting is carried out. In the numerical simulation, a rock model for validation is shown in Figure 3, which is simplified to a plane strain model. The size of the rock model is 0.315 m × 0.285m. The radius of the borehole is 3 mm. The rock adopts the linear elastic constitutive model, the explosive adopts the Landau model, the interface between the rock elements adopts the fracture energy model, and the boundary is set as the non-reflection boundary condition. The rock material parameters are shown in Table 1, the explosive parameters shown in Table 2, and the basic parameters of the interface shown in Table 3.

Figure 4a shows the cracks distribution of single-borehole blasting calculated by the original CDEM method, while Figure 4b shows that calculated by the improved CDEM method. It can be found that there are obvious differences in the number of main cracks obtained by two calculation methods. The number of main cracks obtained by the original CDEM method is more than 10, while the number obtained by the improved CDEM method is about 8. As shown in Figure 5, the experimental result of rock blasting model shows that the number of main cracks in single-borehole blasting is generally 5–8. The circumferential crack in Figure 5 is caused by the reflected wave, a tensile wave, at the boundary. There is no circumferential crack in Figure 4, because the boundary is a non-reflection boundary. It is obvious that the number and distribution of cracks calculated by the improved CDEM method are more close to practical results.

3. Effects of in-situ stresses on the distribution of blast-induced cracks

To study the effect of in-situ stresses on the distribution of blast-induced cracks, numerical simulations of single-borehole blasting at the uniaxial in-situ stress, biaxial equal in-situ stress and biaxial unequal in-situ stress conditions are respectively carried out. According to different in-situ stress conditions, different horizontal in-situ stresses σ_h and vertical in-situ stresses σ_v are applied to the model with the same model size and other relevant parameters as the above verification case. There are many numerical simulation cases in the following paragraphs. For the convenience of description, the in-situ stress condition is represented of σ_h-σ_v. For example, 5–10 means the horizontal in-situ stress is 5 MPa and the vertical in-situ stress is 10 MPa.

3.1. Uniaxial in-situ stress

In order to study the distribution of blast-induced cracks at the uniaxial in-situ stress condition, horizontal in-situ stress σ_h=0MPa and vertical in-situ stress σ_v>0MPa are applied to the model. Figure 6 shows the distribution of blast-induced cracks under different uniaxial in-situ stress conditions. Figure 6a shows that the blast-induced cracks are omnidirectional when in-situ stresses are zero. As shown in Table 4, with the increase of vertical in-situ stress σ_v, the distribution of blast-induced cracks has a significantly variation in the quantity of main cracks and the length of the longest horizontal crack. The quantity of main cracks decreases with the increase of vertical in-situ stress σ_v, and the main horizontal crack gradually shortens. When the vertical in-situ stress $\sigma_v \geq$15MPa, the horizontal main crack doesn't appear anymore. It can be seen that the vertical in-situ stress significantly inhibits the propagation of the horizontal crack. In addition, with the increase of the vertical in-situ stress σ_v, the main crack obviously tends to propagate in the vertical direction, which verifies the guiding effect of the in-situ stress.

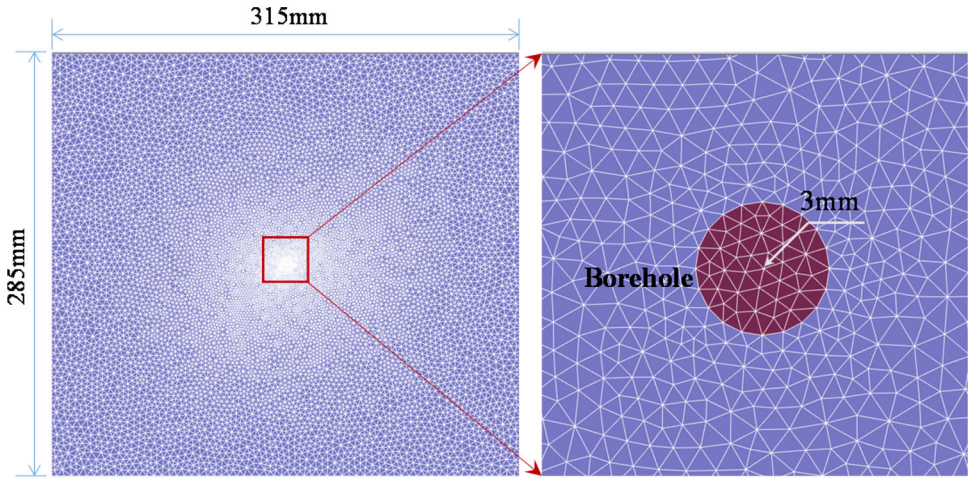

Figure 3. Model size and meshing.

Table 1. Basic parameters of rock.

Density/kg·m^{-3}	Elastic modulus/GPa	Compressive strength/MPa	Velocity of longitudinal wave/m·s^{-1}	Poisson's ratio	Cohesion/MPa	Tensile strength/MPa	Internal friction angle/°	Dilation angle/°
1466	6.1	30	3500	0.31	3	1	40	10

Table 2. Basic parameters of explosive.

Detonation velocity/m·s^{-1}	Detonation heat /J·kg^{-1}	Adiabatic index in the initial stage	Adiabatic index in the second stage	Detonation pressure/MPa
5000	3100	3.0	1.333	7000

Table 3. Basic parameters of interface.

Normal/tangential stiffness/GPa	Friction angle/°	Cohesion/GPa	Tensile strength/MPa
5×10^5	40°	20	10

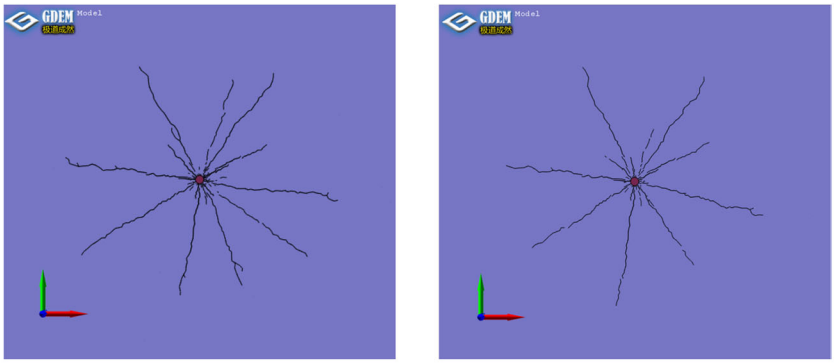

(a) Calculated by the original CDEM method (b) Calculated by the improved CDEM method

Figure 4. The cracks distribution in numerical simulation of single-borehole blasting.

3.2. Biaxial equal in-situ stress

In order to study the distribution of blast-induced cracks at the biaxial equal in-situ stress condition, biaxial equal in-situ stresses ($\sigma_h = \sigma_v$) are applied to the model. Figure 7 shows the distribution of blast-induced cracks at different biaxial equal in-situ stress conditions. The quantity of main cracks and the length of the longest crack at different biaxial equal in-situ stress conditions are shown in Table 5. It is clear that with the increase of in-situ stresses, the number of main cracks is always 8, while the length of the main cracks decreases. When there is no in-situ stress, the length of longest horizontal main crack is 104 mm, and the length of longest vertical main crack is 99 mm. When the biaxial equal in-situ stress is 10 MPa, the lengths of longest horizontal main crack and longest vertical main crack are both 19 mm. It can be seen that the biaxial equal in-situ stresses inhibit the propagation of blast-induced cracks in all directions. Moreover, the inhibition effect is significantly strengthened with the increase of in-situ stresses. In addition, at the biaxial equal in-situ stress condition, the length of horizontal crack is basically the same as that of vertical crack. At the same time, the crack propagation has no obvious directionality, indicating that biaxial equal in-situ stresses have no guiding effect on the propagation of blast-induced cracks.

3.3. Biaxial unequal in-situ stress

In order to study the distribution of blast-induced cracks at the biaxial unequal in-situ stress condition, different biaxial in-situ stresses are applied to the model. To facilitate the comparative analysis, the stress difference between the vertical in-situ stress σ_v and the horizontal in-situ stress σ_h is both 5 MPa. Figure 8 shows the distribution of blast-induced cracks at different biaxial unequal in-situ stress conditions. The number of main cracks and the lengths of the longest crack at different biaxial unequal in-situ stress conditions are shown in Table 6. It can be found that with the increase of in-situ stress, the lengths of blast-induced cracks in all directions gradually decrease. However, due to the different in-situ stresses in the horizontal direction and vertical direction, there are also differences in the lengths of the horizontal cracks and the vertical cracks in the same numerical simulation case. The propagation of horizontal cracks is mainly inhibited by the vertical in-situ stress. While the propagation of the vertical cracks is mainly inhibited by the horizontal in-situ stress. In the same case, the vertical in-situ stress is larger than horizontal in-situ stress, so the length of the horizontal crack is smaller than that of the vertical crack.

Figure 5. The cracks distribution in model experiment of single-borehole blasting.

4. Effects of in-situ stresses on stress evolution and crack propagation

4.1. Uniaxial in-situ stress

In order to study the blast-induced stress evolution and crack propagation at the uniaxial in-situ stress conditions, numerical simulation cases 0-0, 0-5 and 0-10 are analyzed in

Table 4. The quantity of main cracks and the length of horizontal crack at the uniaxial in-situ stress condition.

Uniaxial in-situ stress	0-0	0-5	0-10	0-15	0-20
Quantity of main cracks	8	6	6	6	5
Length of the longest horizontal crack/mm	104	33	22	0	0

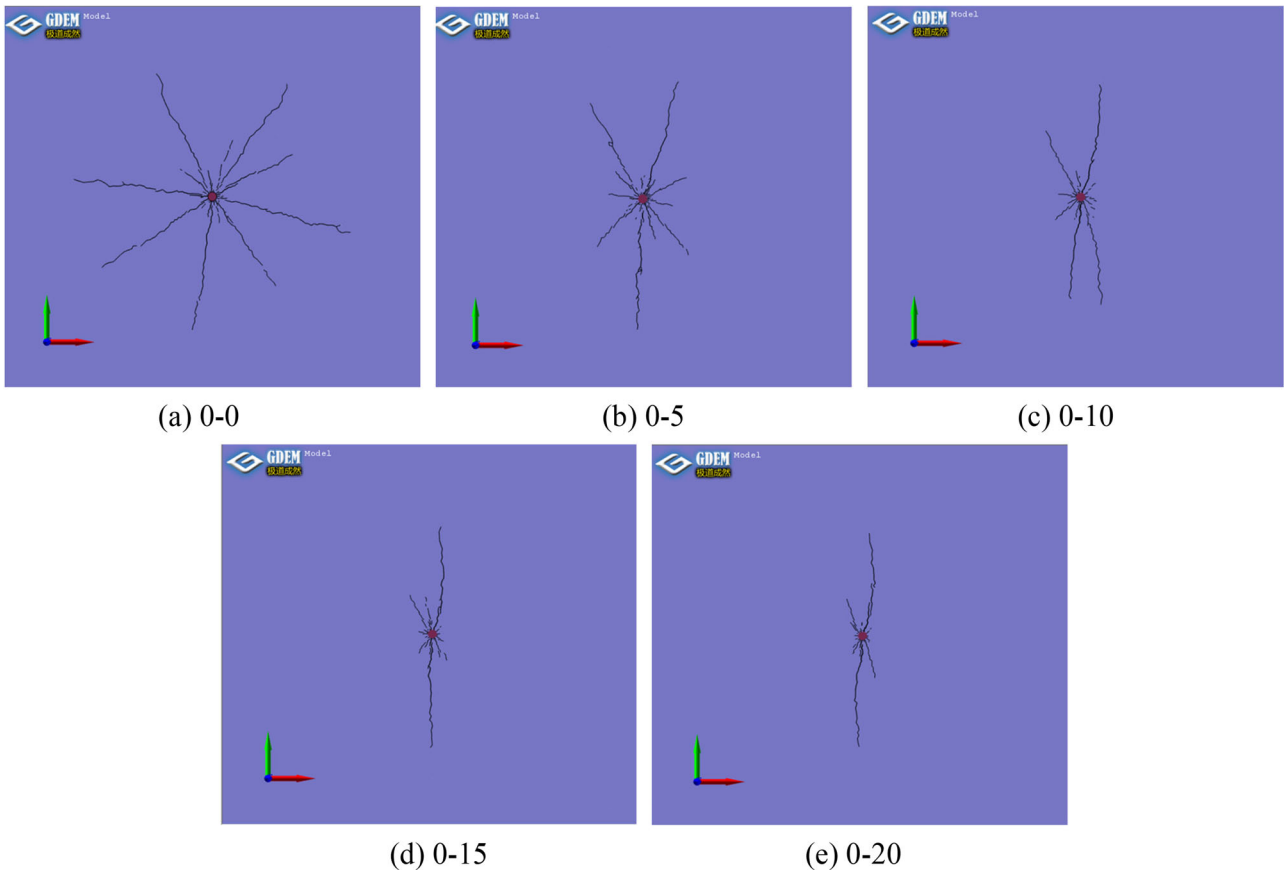

Figure 6. The distribution of blast-induced cracks at the uniaxial in-situ stress condition.

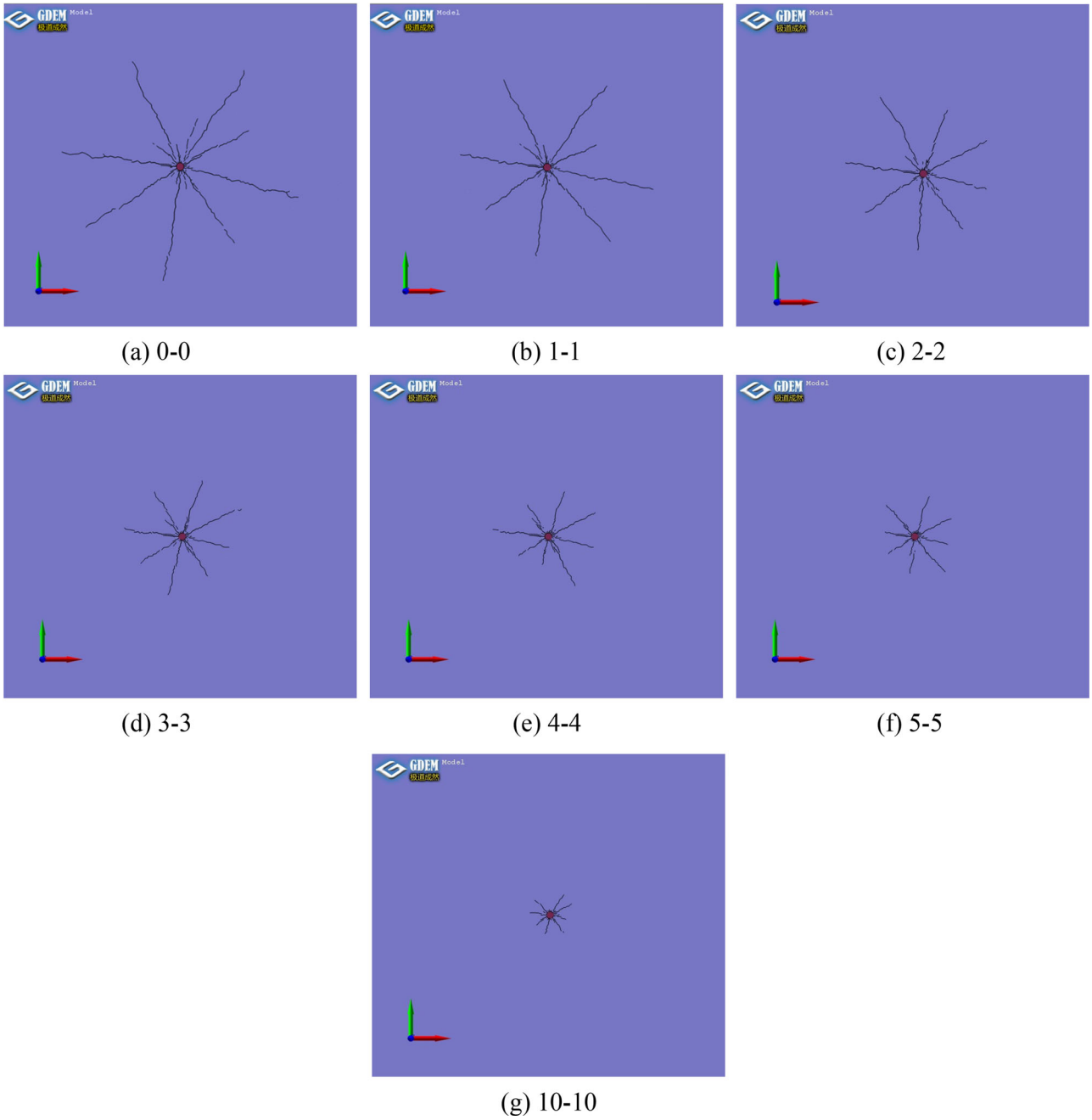

Figure 7. The distribution of blast-induced cracks at the biaxial equal in-situ stress condition.

Table 5. The number of main cracks and the lengths of cracks at the biaxial equal in-situ stress condition.

Biaxial equal in-situ stress	0-0	1-1	2-2	3-3	4-4	5-5	10-10
Quantity of main cracks	8	8	8	8	8	8	8
Length of the longest horizontal crack/mm	104	98	73	67	51	34	19
Length of the longest vertical crack/mm	99	85	67	51	52	40	19

this section. Figure 9 shows the stress evolution and crack propagation at the uniaxial in-situ stress condition. The detonation of the explosive is initiated as $t = 0\mu s$. After the detonation, a number of cracks are formed around the borehole. Some of them become the main cracks in the subsequent propagation process, while the rest stop due to insufficient propagation energy. The in-situ stress has no effect on the stress evolution and crack propagation in case 0-0. The stress wave propagates outward with the circular wavefront centered at the borehole. As a result, the propagation direction of the crack is random. Nevertheless, the stress evolution and crack propagation are affected by the in-situ stresses in case 0-5 and 0-10. The stress wave propagates outward with the elliptical wavefront centered on the borehole. The propagation of blast-induced cracks is directional. In particular, the horizontal crack propagation is suppressed. The larger the vertical in-situ stress σ_v, the more significant the effect on the stress wave evolution and crack propagation.

As shown in Figure 10, relevant gauging points are selected for stress analysis. Specifically, the horizontal

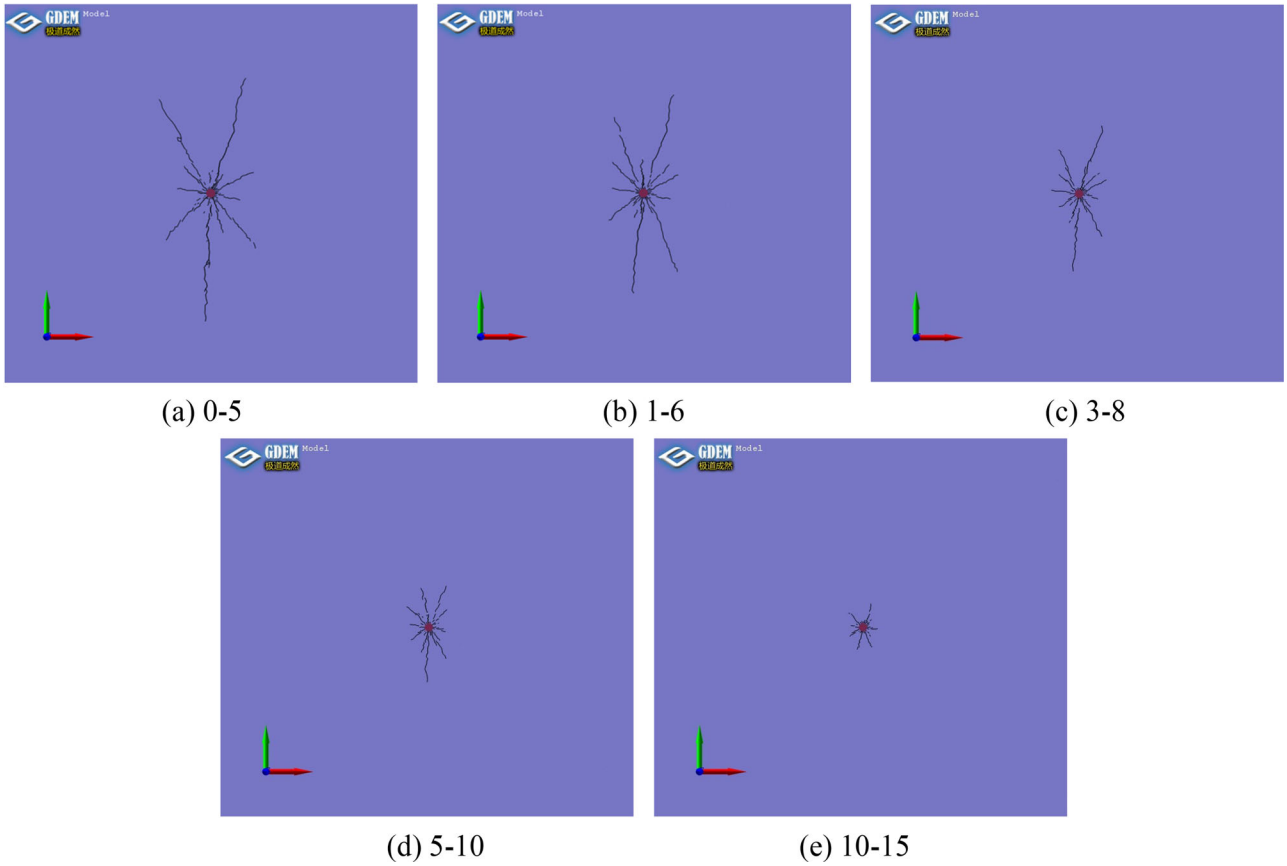

Figure 8. The distribution of blast-induced cracks at the biaxial unequal in-situ stress condition.

Table 6. The number of main cracks and the lengths of cracks at the biaxial unequal in-situ stress condition.

Biaxial unequal in-situ stress	0-5	1-6	3-8	5-10	10-15
Number of main cracks	6	8	8	8	6
Length of the longest horizontal crack/mm	33	30	20	20	9
Length of the longest vertical crack/mm	101	80	52	26	14

gauging points H1, H2, H3, H4 and H5 are selected. The distance of gauging point H1 from the borehole is 20 mm, and the distance between two adjacent gauging points is 20 mm. Similarly, the vertical gauging points V1, V2, V3, V4 and V5 are selected. The distance of gauging point V1 from the borehole is 20 mm, and the distance between two adjacent gauging points is 20 mm. The following description mainly analyzes the radial stress σ_r and circumferential stress σ_θ of the relevant gauging points.

Under the blasting load, the radial stress σ_r of the gauging point is mainly compressive. At the same time, the circumferential stress σ_θ gradually changes from compressive stress to tensile stress, and is mainly tensile stress in the whole process [30]. Figure 11 shows the stress evolution curves of vertical gauging points in case 0-0. It is indicated that the stress states of both horizontal and vertical gauging points with the same distance to borehole are the same in case 0-0. It can be seen from the figure that the stress variation trends at different gauging points are basically the same. The blasting stress gradually attenuates with the increase of the distance from the borehole, so the stress peak value of the corresponding gauging point gradually decreases.

Figures 12 and 13 show the stress evolution curves of horizontal and vertical gauging points in case 0–5 respectively. It is obvious that the stress wave characteristics of the gauging points are very similar to those in case 0-0. The preliminary comparison shows that the stress peak value evolution of the vertical gauging points and that of the horizontal gauging points are apparently different. It is indicated that such in-situ stress condition has different effects of stress evolution on the gauging points in different directions.

Figure 14 shows the variation of the stress peak in the three cases (0-0, 0-5, 0-10) at the uniaxial in-situ stress condition. It can be found that the in-situ stress has significant effect on the variation of the stress peak. The in-situ stress significantly increases the radial stress peak of the vertical gauging points, but significantly reduces the radial stress peak of the horizontal gauging points. This effect can be strengthened by the increase of in-situ stress. Besides, the in-situ stress has no obvious effect on the circumferential stress peak of the vertical gauging points, but significantly reduces the circumferential stress peak of the horizontal gauging points. With the increase of the in-situ stress and the distance from the borehole, the circumferential stress of the horizontal gauging points gradually changes from tensile stress to compressive stress. This means the stress states are changed by the action of the in-situ stress. As it is well known, the radial cracks under blasting load are mainly caused by circumferential tensile stress. It can be seen that, from the stress state of the gauging point, the vertical in-situ

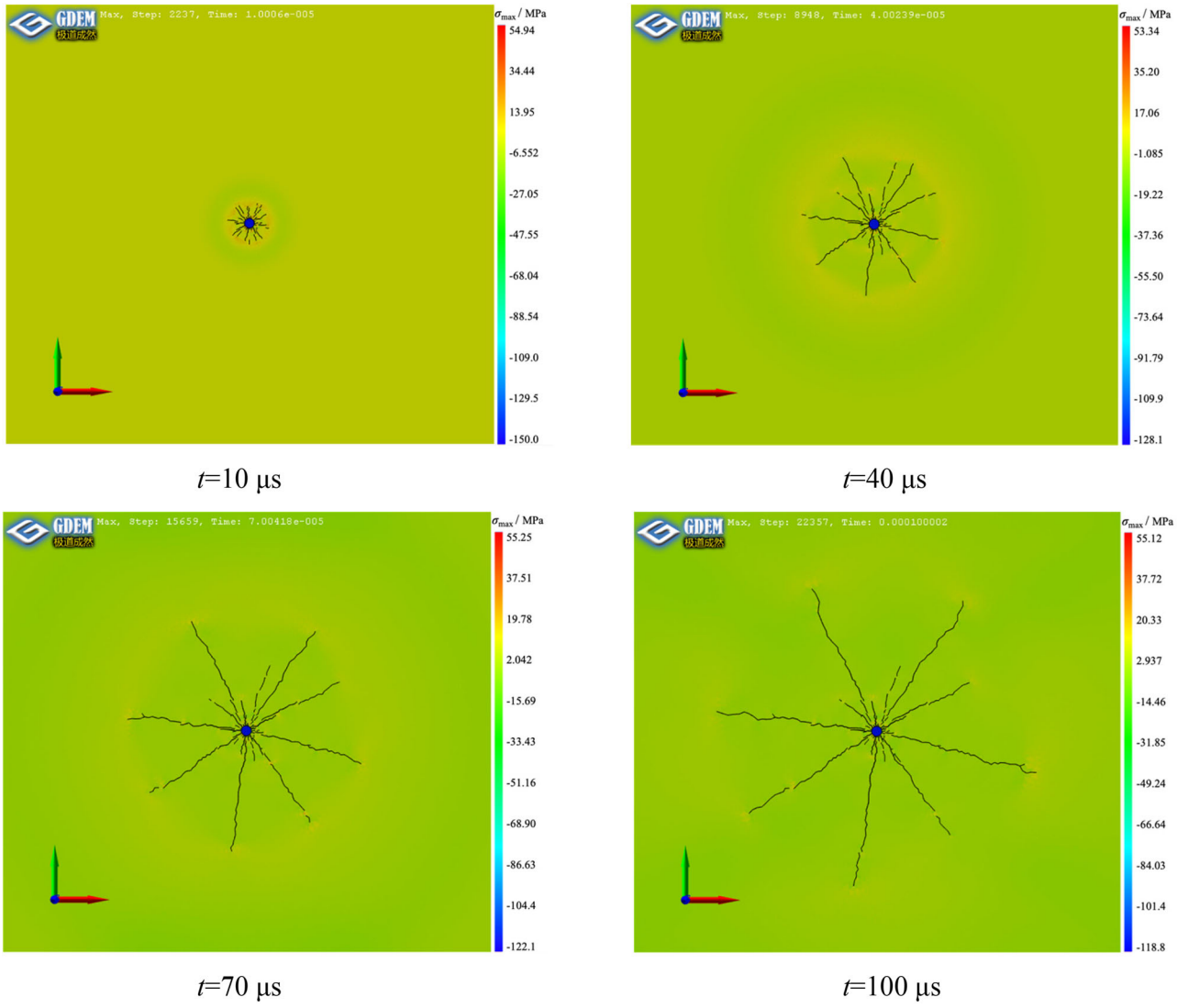

(a) 0-0

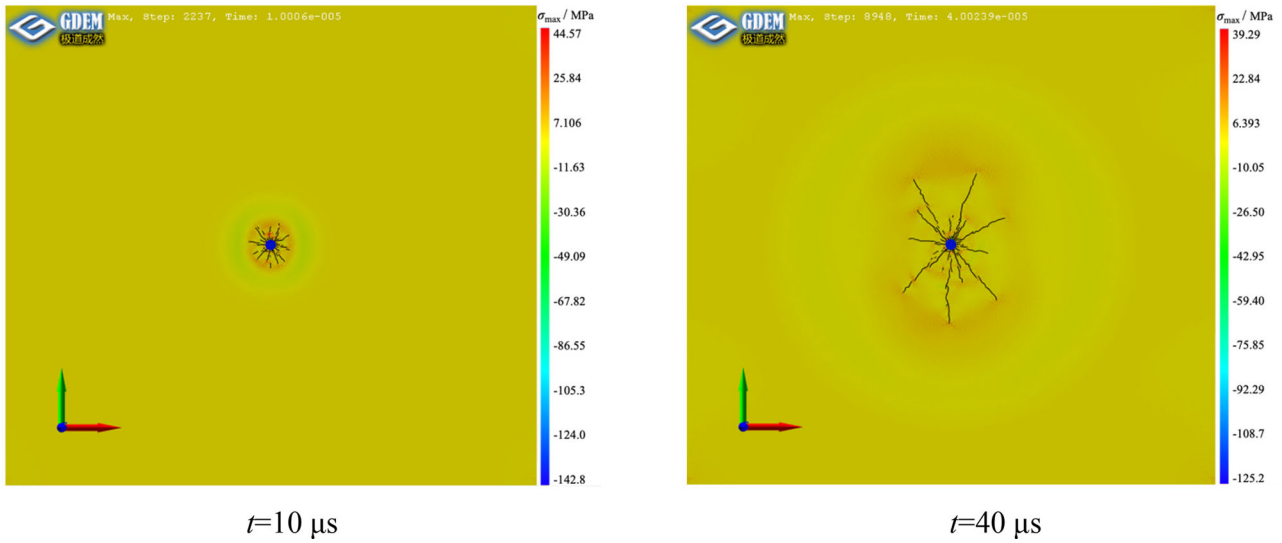

Figure 9. Evolution of the maximum principal stress and blast-induced crack propagation process at the uniaxial in-situ stress condition.

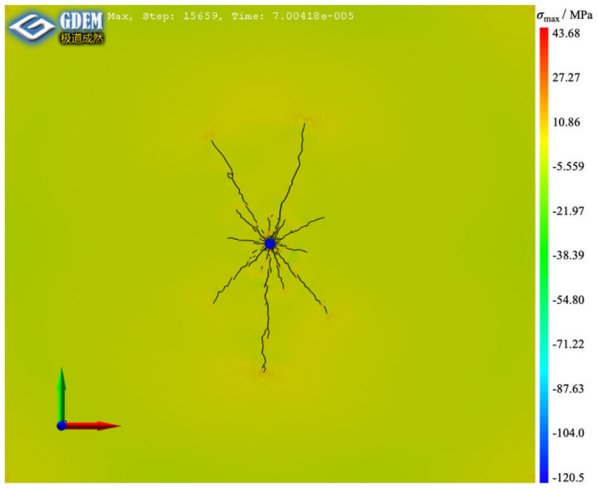

t=70 μs

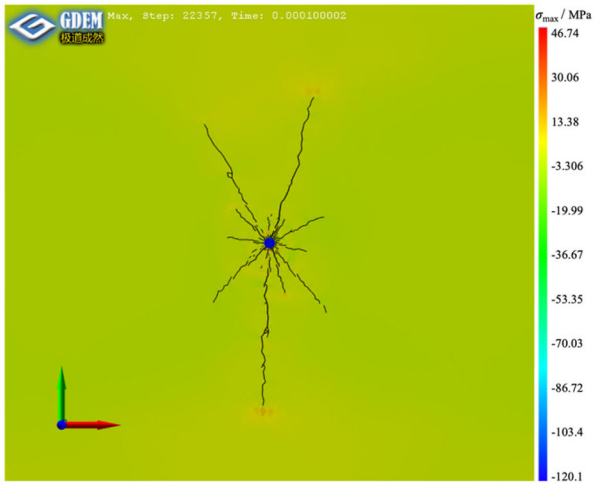

t=100 μs

(b) 0-5

t=10 μs

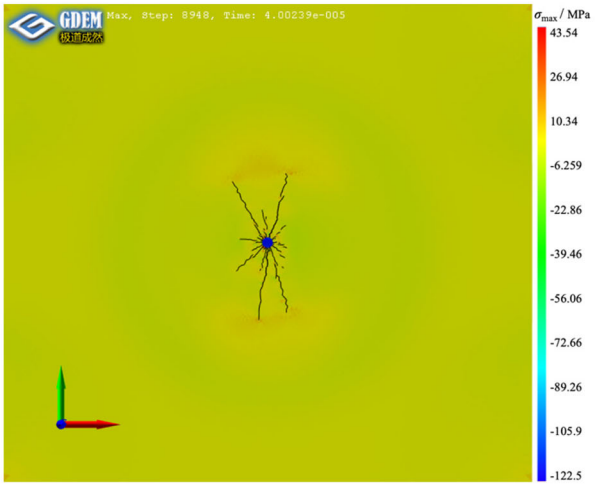

t=40 μs

t=70 μs

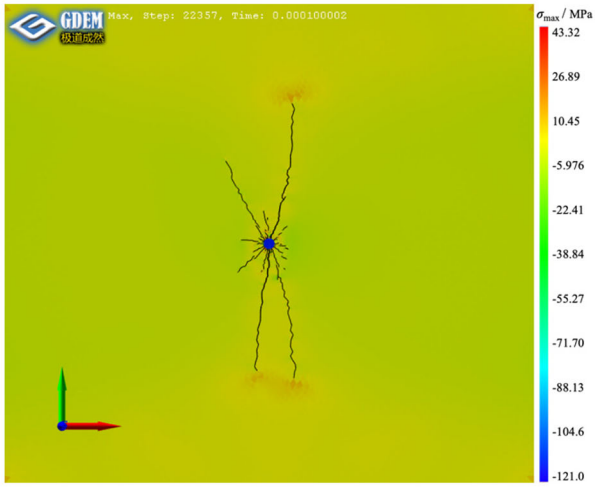

t=100 μs

(c) 0-10

Figure 9. Continued.

stress will significantly inhibit the propagation of the horizontal crack. Such inhibitory effect will increase with the increase of the in-situ stress.

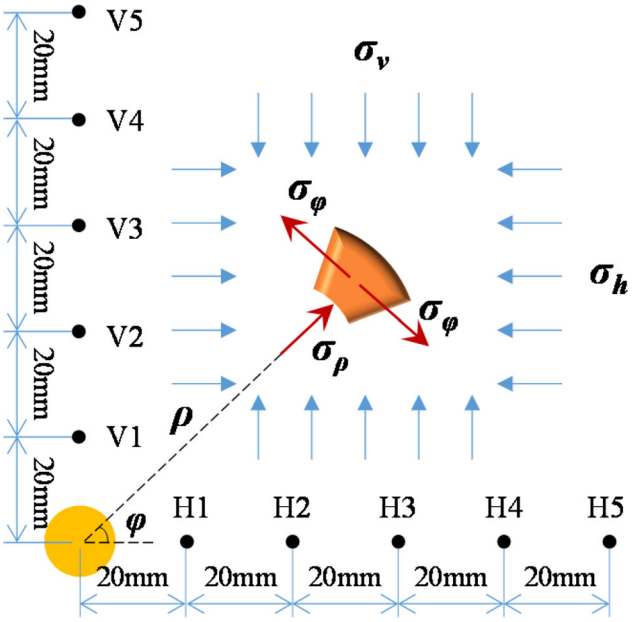

Figure 10. Diagram of the gauging point and borehole positions.

On this basis, the dynamic stress evolution of the crack tip in the horizontal and vertical directions is further analyzed below. The longest cracks in the horizontal and vertical directions are selected for this analysis. Figure 15 shows the variation of the maximum principal stress at the crack tip with time in the three cases at the uniaxial in-situ stress condition. When there is no in-situ stress (0-0), the variation trends of the stress at both horizontal and vertical crack tips are basically the same. Under the action of vertical in-situ stress, the variations of stress at horizontal crack tip and vertical crack tip are obviously different, and the stresses at the horizontal crack tip decrease significantly and decay rapidly. In addition, with the increase of vertical in-situ stress, this effect becomes more and more obvious.

4.2. Biaxial equal in-situ stress

In order to study the stress evolution and crack propagation at the biaxial equal in-situ stress condition, case 5-5 and case 10-10 are studied in this section. Figure 16 shows the stress evolution and crack propagation in the two cases. The figure also indicates that the biaxial equal in-situ stresses have strengthened the inhibitory action on the propagation of both horizontal and vertical cracks. The crack propagation has remarkable variation compared with that at the

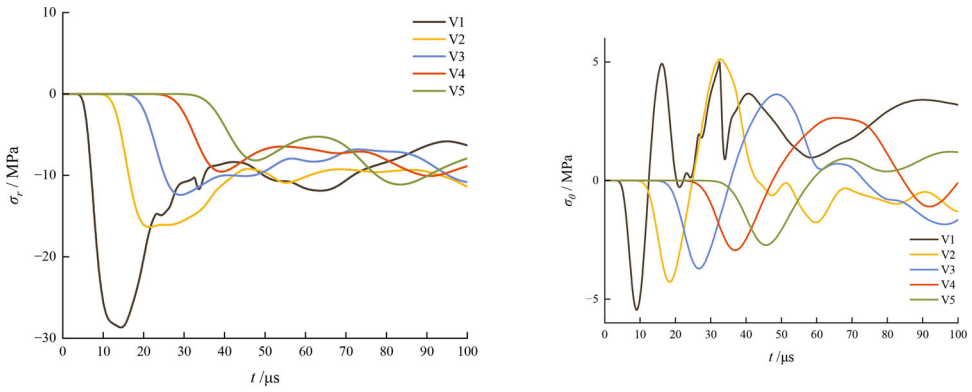

(a) Radial stress σ_r (b) Circumferential stress σ_θ

Figure 11. Stress evolution curves of gauging points in case 0-0.

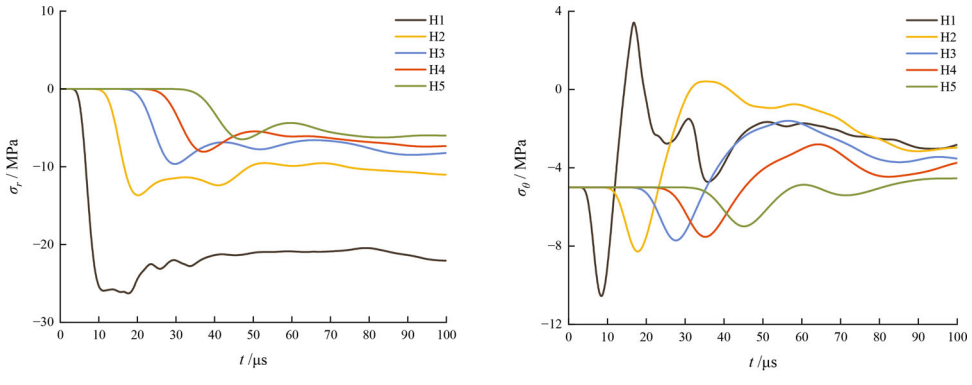

(a) Radial stress σ_r (b) Circumferential stress σ_θ

Figure 12. Stress component of horizontal gauging points vs. time in case 0–5.

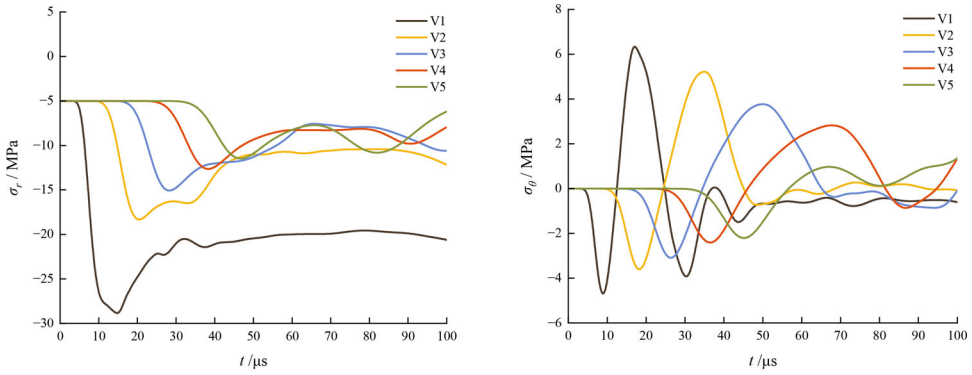

(a) Radial stress σ_r (b) Circumferential stress σ_θ

Figure 13. Stress component of vertical gauging points vs. time in case 0–5.

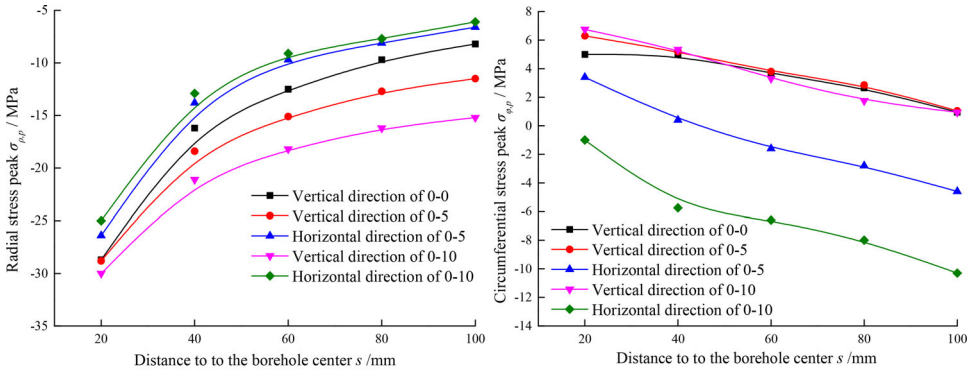

(a) Radial stress peak $\sigma_{r,p}$ (b) Circumferential stress peak $\sigma_{\theta,p}$

Figure 14. Variation law of stress peak value for the three cases at the uniaxial in-situ stress condition.

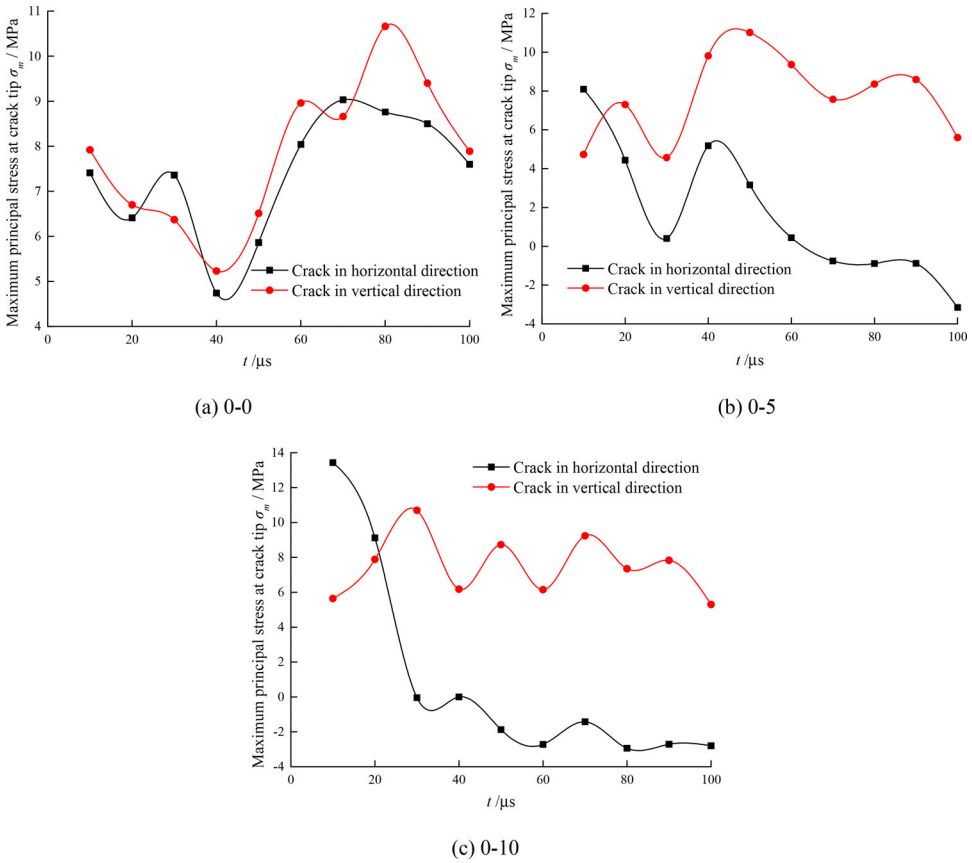

(a) 0-0 (b) 0-5

(c) 0-10

Figure 15. Maximum principal stress σ_m at crack tip vs. time in the three cases at the uniaxial in-situ stress condition.

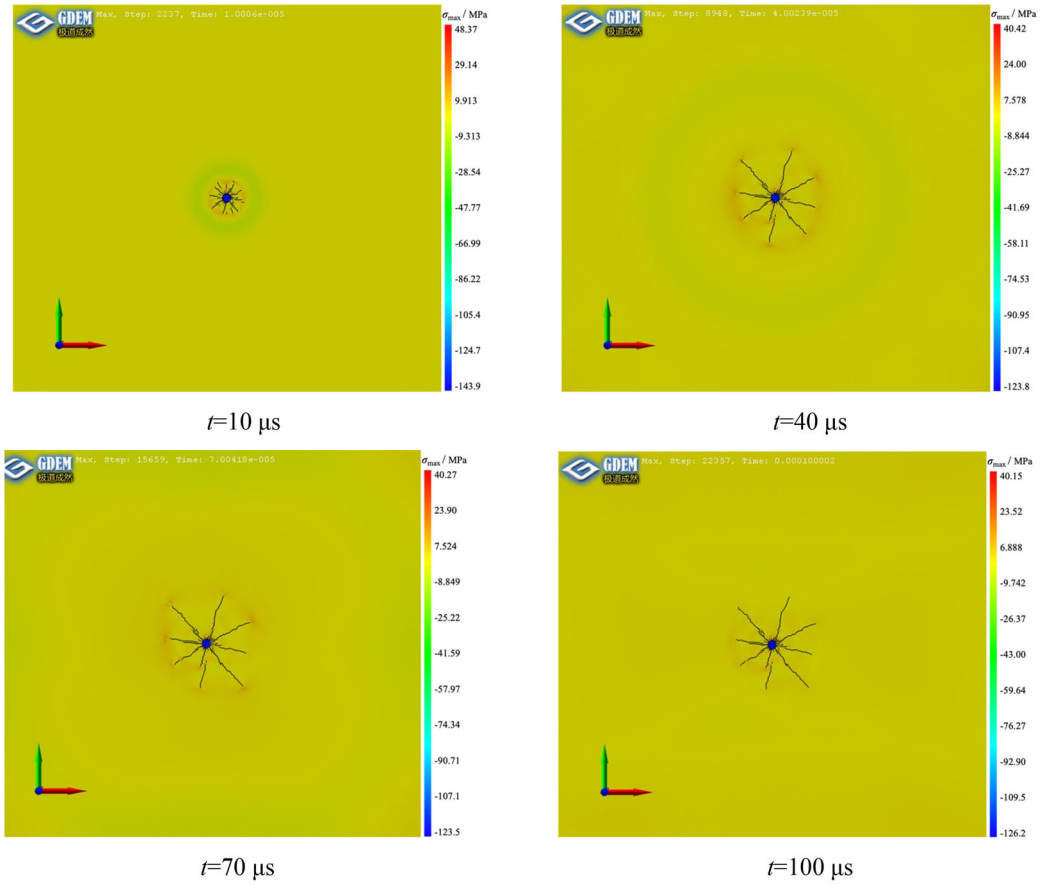

(a) 5-5

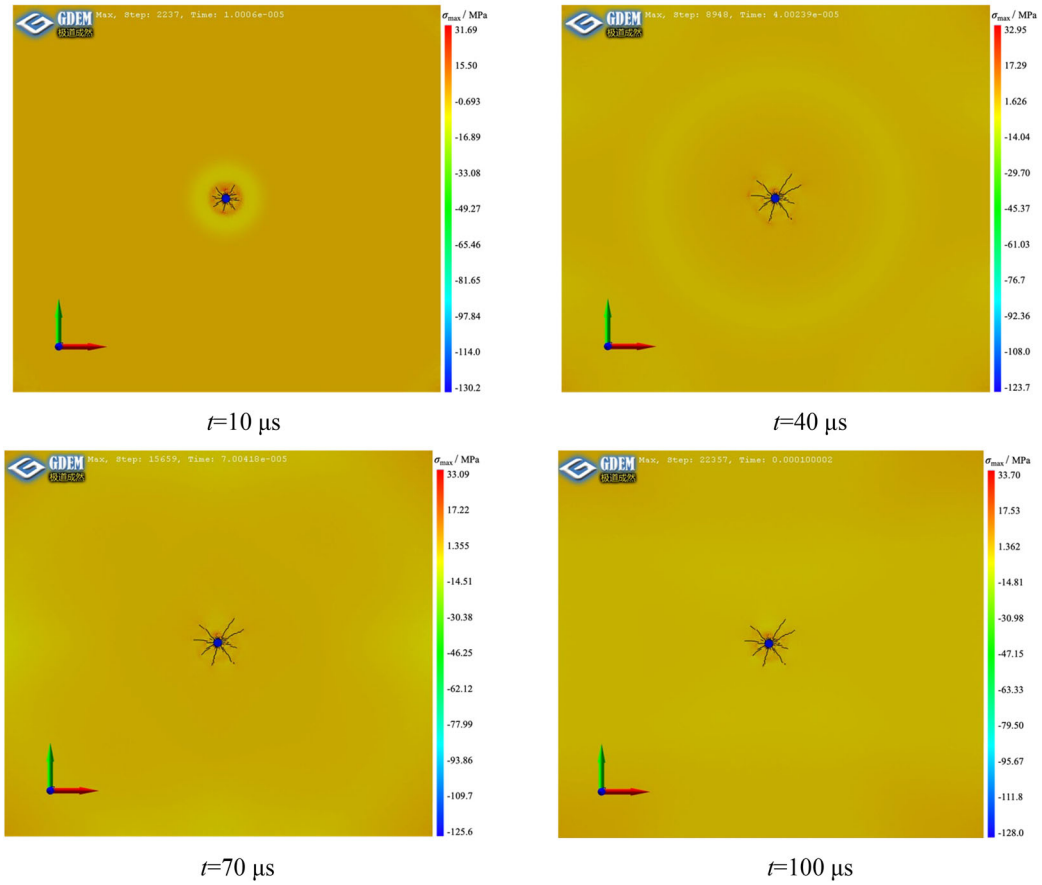

(b) 10-10

Figure 16. Evolution of the maximum principal stress and blast-induced crack propagation process at the biaxial equal in-situ stress condition.

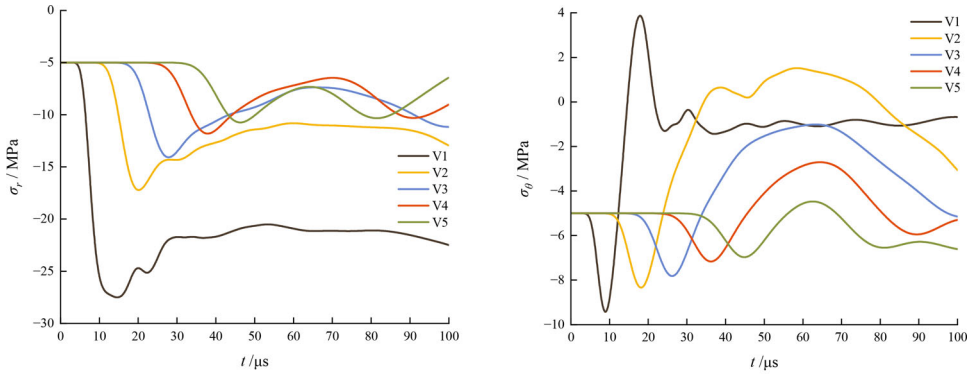

(a) Radial stress σ_r (b) Circumferential stress σ_θ

Figure 17. Stress component of vertical gauging points vs. time in case 5-5.

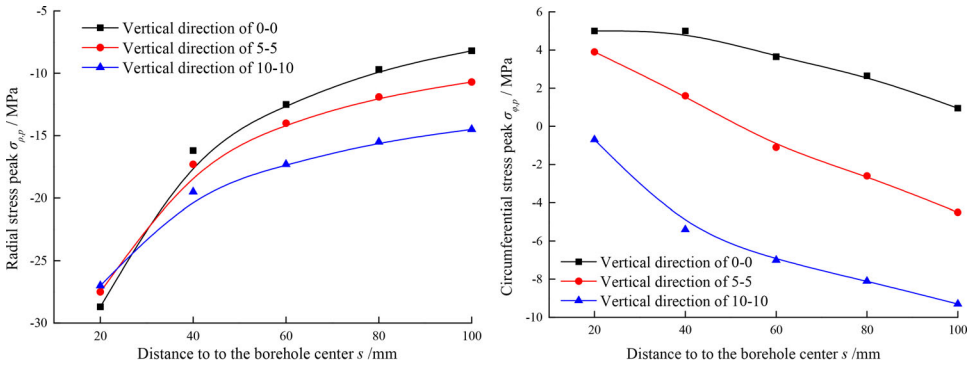

(a) Radial stress peak $\sigma_{r,p}$ (b) Circumferential stress peak$\sigma_{\theta,p}$

Figure 18. Variation law of stress peak value for the three cases at the biaxial equal in-situ stress condition.

uniaxial in-situ stress condition. It is clear that different in-situ stress states have different effects on the propagation of blast-induced cracks.

Because the gauging points have the same stress states in both horizontal direction and vertical direction of the borehole at the biaxial equal in-situ stress condition, it is enough to select the gauging points in the vertical direction for analysis. Figure 17 shows the stress evolution curve of the vertical gauging points of case 5-5. Affected by the in-situ stress, the initial radial stress and the initial circumferential stress of the measuring point are both 5 MPa. The stress evolution trend is basically the same as that without in-situ stress.

Figure 18 shows the variation of the stress peak the in three cases (0-0, 5-5, 10-10) at the biaxial equal in-situ stress condition. It can be found that both the radial stress and the circumferential stress gradually decrease with the increase of the in-situ stress. In particular, with the increase of the in-situ stress, the circumferential stress state of the gauging point gradually changes from tension to compression. The results are basically consistent with previous research [11, 14], and further comparative analysis of the stress at different positions of rock mass.

4.3. Biaxial unequal in-situ stress

Figure 19 shows the stress evolution and crack propagation of the two cases. The figure also indicates that the biaxial unequal in-situ stress has varying degrees of inhibitory action on both the horizontal and vertical cracks, compared with the case 0-0. The crack propagation in the horizontal direction is mainly affected by the vertical in-situ stress, while the crack propagation in the vertical direction is mainly affected by the horizontal in-situ stress. In case 5-10 and case 10-15, the vertical in-situ stress is greater than the horizontal in-situ stress, resulting in relatively short horizontal cracks.

Figures 20 and 21 show the stress evolution curves of the gauging points in the horizontal and vertical directions of the case 5–10. Under the action of biaxial unequal in-situ stress, the stress evolution trend and the stress value of the gauging points in the horizontal and vertical directions are different. From this, the stress peaks of different gauging points in case 5-10 and case 10-10 are extracted for analysis, compared with the case 0-0. As Figure 22 shows, at the biaxial unequal in-situ stress condition, both the radial stress and the circumferential stress peak of the gauging points are significantly reduced. Such effect can be strengthened with the increase of in-situ stress. Moreover, the circumferential stress characteristic of the gauging points transitions from tension to compression with the increase of the in-situ stress.

The results of this study are basically consistent with the previous studies [10, 15], and the stress situation is further explored on the basis of the crack distribution study. In

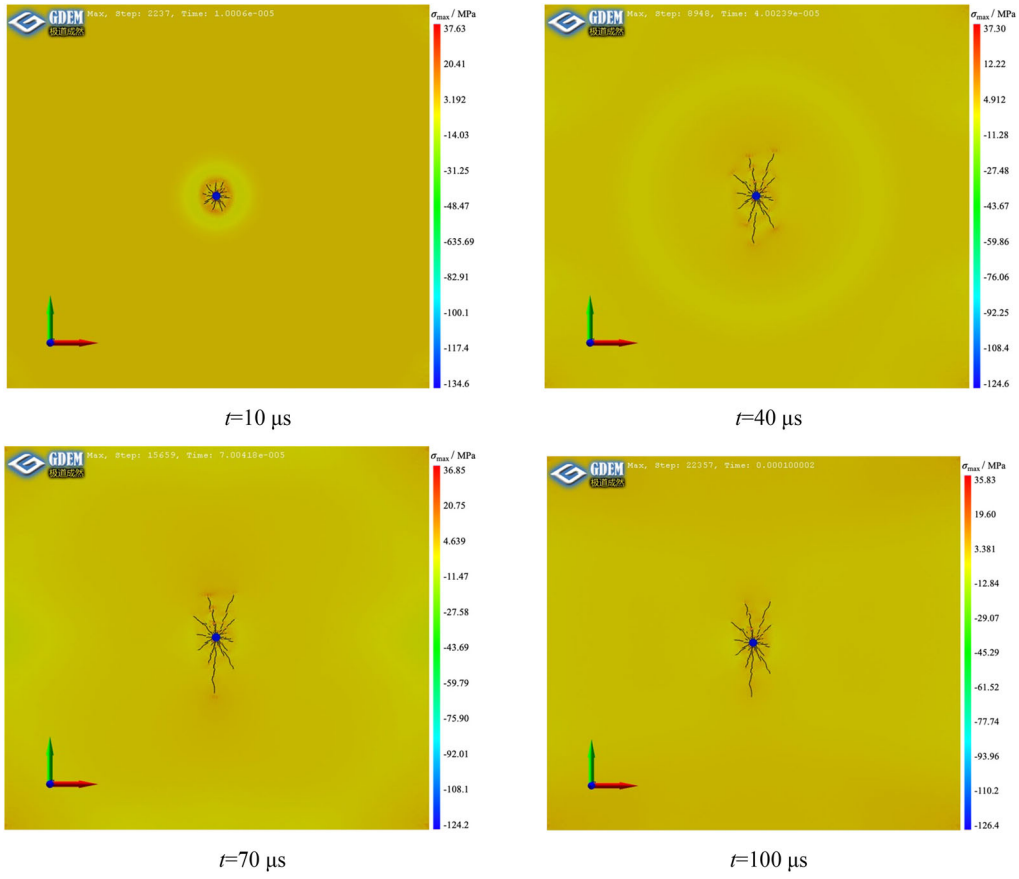

(a) 5-10

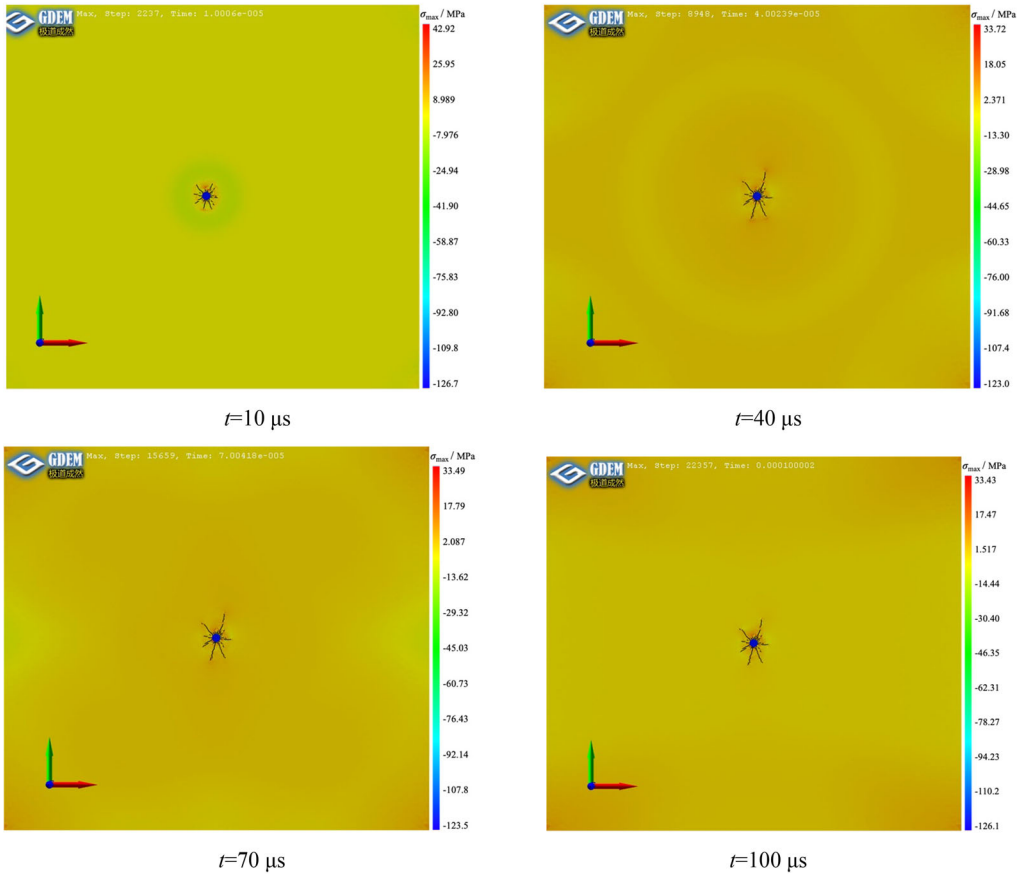

(b) 10-15

Figure 19. Evolution of the maximum principal stress and blast-induced crack propagation process at the biaxial unequal in-situ stress condition.

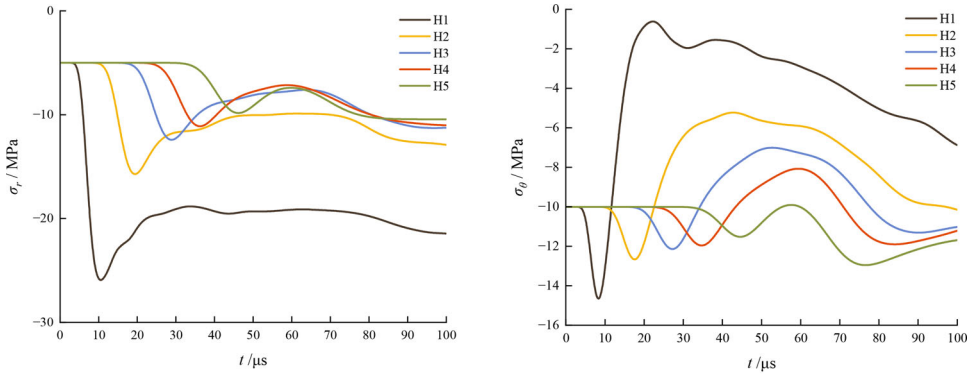

(a) Radial stress σ_r (b) Circumferential stress σ_θ

Figure 20. Stress component of horizontal gauging points vs. time in case 5–10.

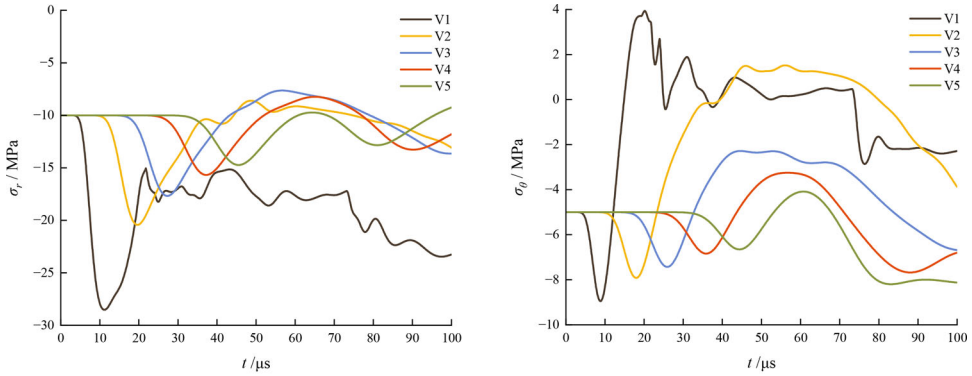

(a) Radial stress σ_r (b) Circumferential stress σ_θ

Figure 21. Stress component of vertical gauging points vs. time in case 5–10.

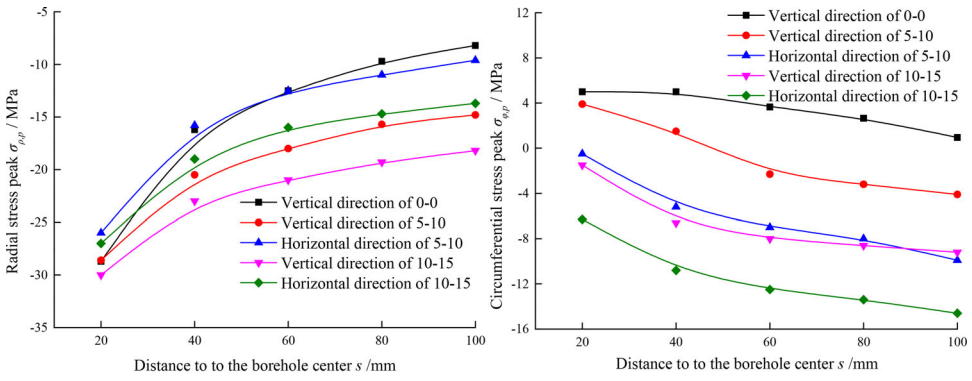

(a) Radial stress peak $\sigma_{r,p}$ (b) Circumferential stress peak $\sigma_{\theta,p}$

Figure 22. Variation law of stress peak value for the three cases at the biaxial unequal in-situ stress condition.

practical engineering, vertical stress and horizontal stress are often inconsistent. The study in this section on the influence of biaxial unequal in-situ stress on crack propagation is very meaningful to a more comprehensive understanding of the influence of in-situ stress on blasting cracks.

5. Conclusion and discussion

In this study, an improved CDEM method with the calculation plug-in of the energy consumption considering the energy consumption of the crushed zone under blasting load is used to carry out the numerical simulation study of the blast-induced crack propagation at different in-situ stress conditions. It is found that the in-situ stress has a significant effect on the distribution of cracks, the evolution law of blasting stress and the propagation process of blast-induced cracks. The relevant conclusions are as follows:

1. Uniaxial in-situ stress: Under the action of vertical in-situ stress, the tip stress of horizontal crack decreases

significantly and decays rapidly. With the increase of vertical in-situ stress, such effect becomes more and more obvious. The propagation of the horizontal blast-induced crack is significantly inhibited. In addition, with the increase of the in-situ stress, the main blast-induced cracks obviously tend to expand in the vertical direction, which verifies the guiding effect of the in-situ stress. Under the action of vertical in-situ stress, the propagation process of blasting stress changes. The blasting stress propagates outward through an elliptical wavefront centered on the borehole. The in-situ stress significantly increases the radial stress peak value of the vertical gauging points, but significantly reduces the radial stress peak value of the horizontal gauging points. While the in-situ stress has no obvious effect on the circumferential stress peak value of the vertical gauging points, but significantly reduces the circumferential stress peak value of the horizontal gauging points.

2. Biaxial equal in-situ stress: Under the action of biaxial equal in-situ stress, the propagation of cracks in both the horizontal and vertical directions is significantly inhibited. The crack propagation process is significantly different from that under the action of uniaxial in-situ stress. Both of the peak values of radial stress and circumferential stress of the gauging points decrease gradually with the increase of in-situ stress. In particular, the circumferential stress states of the gauging points gradually change from tension to compression with the increase of the in-situ stress.
3. Biaxial unequal in-situ stress: Under the action of biaxial unequal in-situ stress, there are different inhibitions on crack propagation in the horizontal direction and the vertical direction. Both the radial stress peak and the circumferential stress peak of the gauging points decrease significantly. Such effect becomes more significant with the increase of the in-situ stress.

It is generally accepted that the blast-induced crack propagation is resultant from the two distinct loading phases of rock blast, that is, the stress wave propagation and the gas pressurization. However, the gas pressurization phase is too complex to be considered in this in this study provisionally. It is urgent to study the numerical calculation method which strictly considers the actual interaction process of gas pressurization and stress wave propagation.

Disclosure statement of competing interest

The authors declare that they have no conflicts of interest to this work. The authors declare that they do not have any commercial or associative interest that represents a conflict of interest in connection with the work submitted.

Funding

This research was supported by: (1) National Natural Science Foundation of China (52204085, 51934001); (2) Interdisciplinary Research Project for Young Teachers of USTB (Fundamental Research Funds for the Central Universities) (FRF-IDRY-21-006); (3) Fundamental Research Funds for the Central Universities (QNXM20220010); (4) Foundation of Hubei Key Laboratory of Blasting Engineering (BL2021-05).

References

[1] Z.X. Zhang, D.F. Hou, A. Aladejare, T. Ozoji, and Y. Qiao, World mineral loss and possibility to increase ore recovery ratio in mining production, Int. J. Min. Reclam. Environ., vol. 35, no. 9, pp. 670–691, 2021. DOI: 10.1080/17480930.2021.1949878.

[2] M.C. He, H.P. Xie, S.P. Peng, and Y.D. Jiang, Study on rock mechanics in deep mining engineering, Chin. J. Rock Mech. Eng., vol. 24, no. 16, pp. 2803–2813, 2005. [in Chinese]

[3] Y.T. Zhang, R.S. Yang, C. Chen, C.X. Li, and H.H. Luo, Analysis of the blasting effect of strip cartridge position on jointed rock mass, Mech. Adv. Mater. Struct., vol. 30, no. 6, pp. 1249–1259, 2023. DOI: 10.1080/15376494.2022.2029982.

[4] X.P. Li, M. Xu, Y. Wang, G. Wang, J. Huang, W. Yin, and G. Yan, Numerical study on crack propagation of rock mass using the time sequence controlled and notched blasting method, Mech. Adv. Mater. Struct., vol. 26, no. 13, pp. 6714–6732, 2022. DOI: 10.1080/19648189.2021.1956597.

[5] C.X. Ding, C. Xiao, J. Chen, C. Zheng, G. Zhang, S. You, S. He, W. Chen, and X. Liang, Influence of stress waves on the propagation behavior of main crack induced by the slotted cartridge blasting, Mech. Adv. Mater. Struct., pp. 1–7, 2022. (online). DOI: 10.1080/15376494.2022.2116756.

[6] E.T. Brown, and E. Hoek, Trends in relationships between measured in-situ stresses and depth, Int. J. Rock Mech. Min. Sci., vol. 15, no. 4, pp. 211–215, 1978. DOI: 10.1016/0148-9062(78)91227-5.

[7] C.Q. Zhang, G.J. Cui, H. Zhou, F.J. Yang, and J.J. Lu, Influence of mountain-valley morphology on in-situ stress distribution, J. Mt. Sci., vol. 18, no. 9, pp. 2447–2459, 2021. DOI: 10.1007/s11629-020-6228-7.

[8] J.L. Zhao, D.Z. Tang, W.J. Lin, Y. Qin, and H. Xu, In-situ stress distribution and its influence on the coal reservoir permeability in the Hancheng area, eastern margin of the Ordos Basin, China, J. Nat. Gas Sci. Eng., vol. 61, pp. 119–132, 2019. DOI: 10.1016/j.jngse.2018.09.002.

[9] P. Yuan, and Y. Xu, Experimental study on unloading effect of drill and blast excavation in high axial geostress, Fresenius Environ. Bull., vol. 28, no. 11, pp. 7795–7802, 2019.

[10] R.S. Yang, C.X. Ding, Y.L. Li, L.Y. Yang, and Y. Zhao, Crack propagation behavior in slit charge blasting under high static stress conditions, Int. J. Rock Mech. Min. Sci., vol. 119, pp. 117–123, 2019. DOI: 10.1016/j.ijrmms.2019.05.002.

[11] L.Y. Yang, C.X. Ding, R.S. Yang, Z. Lei, and J. Wang, Full field strain analysis of blasting under high stress condition based on digital image correlation method, Shock Vib., vol. 2018, pp. 1–7, 2018. DOI: 10.1155/2018/4894078.

[12] C.X. Ding, R.S. Yang, and L.Y. Yang, Experimental results of blast-induced cracking fractal characteristics and propagation behavior in deep rock mass, Int. J. Rock Mech. Min. Sci., vol. 142, pp. 104772, 2021. DOI: 10.1016/j.ijrmms.2021.104772.

[13] H.K. Kutter, and C. Fairhurst, On the fracture process in blasting, Int. J. Rock Mech. Min. Sci., vol. 8, no. 3, pp. 181–202, 1971. DOI: 10.1016/0148-9062(71)90018-0.

[14] L.Y. Yang, R.S. Yang, P. Xu, and Y.W. Song, Experimental study on the effect of initial compression stress field on blast-induced crack behaviors, Journal of China Coal Society., vol. 38, no. 3, pp. 404–410, 2013. [in Chinese]

[15] L.Y. Yang, R.S. Yang, G.L. Qu, and Z. Yufei, Caustic study on blast-induced wing crack behaviors in dynamic-static superimposed stress field, Int. J. Min. Sci. Technol., vol. 24, no. 4, pp. 417–423, 2014. DOI: 10.1016/j.ijmst.2014.05.001.

[16] F.P. Zhang, J.Y. Peng, X. Zhang, and Y.H. Li, Numerical simulation of the effect of in-situ stress on rock blasting, Metal Mine., vol. 12, pp. 15–18, 2015. [in Chinese]

[17] L.X. Xie, W.B. Lu, Q.B. Zhang, Q.H. Jiang, M. Chen, and J. Zhao, Analysis of damage mechanisms and optimization of cut blasting design under high in-situ stresses, Tunnell. Underground Space Technol., vol. 66, pp. 19–33, 2017. DOI: 10.1016/j.tust.2017.03.009.

[18] C.H. Wei, W.C. Zhu, Y. Bai, and L.L. Niu, Numerical simulation on cutting seam cartridge blasting under different in-situ stress conditions, Explos. Shock Waves., vol. 36, no. 2, pp. 161–169, 2016. [in Chinese]

[19] H.Y. Han, D. Fukuda, H. Liu, E.F.Salmi, E. Sellers, T. Liu, and A. Chan, Combined finite-discrete element modelling of rock fracture and fragmentation induced by contour blasting during tunnelling with high horizontal in-situ stress, Int. J. Rock Mech. Min. Sci., vol. 127, no. C, p. 104214, 2020. DOI: 10.1016/j.ijrmms.2020.104214.

[20] H.Y. Han, D. Fukuda, J. Xie, E.F. Salmi, E. Sellers, H. Liu, H. An, and A. Chan, Rock dynamic fracture by destress blasting and application in controlling rockbursts in deep underground, Comput. Geotech., vol. 155, p. 105228, 2023. DOI: 10.1016/j.compgeo.2022.105228.

[21] H.Y. Han, D. Fukuda, H. Liu, E.F.Salmi, E. Sellers, T. Liu, and A. Chan, FDEM simulation of rock damage evolution induced by contour blasting in the bench of tunnel at deep depth, Tunnell. Underground Space Technol. Incorporating Trenchless Technol. Res., vol. 103, p. 103495, 2020. DOI: 10.1016/j.tust.2020.103495.

[22] H.Y. Han, D. Fukuda, H. Liu, E.F. Salmi, E. Sellers, T. Liu, and A. Chan, Combined finite-discrete element modellings of rockbursts in tunnelling under high in-situ stresses, Comput. Geotech., vol. 137, p. 104261, 2021. DOI: 10.1016/j.compgeo.2021.104261.

[23] H.M. An, H.Y. Liu, H.Y. Han, X. Zheng, and X.G. Wang, Hybrid finite-discrete element modelling of dynamic fracture and resultant fragment casting and muck-piling by rock blast, Comput. Geotech., vol. 81, pp. 322–345, 2017. DOI: 10.1016/j.compgeo.2016.09.007.

[24] C.D. Zheng, R. Yang, Q. Li, C. Ding, C. Xiao, Y. Zhao, and J. Zhao, Fractal analysis for the blast-induced damage in rock masses with one free boundary, Mech. Adv. Mater. Struct., pp. 1–15, 2022. (online). DOI: 10.1080/15376494.2022.2134609.

[25] S.H. Li, J.G. Wang, B.S. Liu, and D.P. Dong, Analysis of critical excavation depth for a jointed rock slope using a face-to-face discrete element method, Rock Mech. Rock Eng., vol. 40, no. 4, pp. 331–348, 2007. DOI: 10.1007/s00603-006-0084-9.

[26] Y.N. Wang, M.H. Zhao, S.H. Li, and J.G. Wang, Stochastic structural model of rock and soil aggregates by continuum-based discrete element method, Sci. China., vol. 48, no. S1, pp. 95–106, 2005.

[27] C. Feng, S.H. Li, W.H. Hao, and W. Ge, Numerical simulation for penetrating and blasting process of EPW based on CDEM, J. Vibr. Shock, vol. 36, no. 13, pp. 11–18, 2017. [in Chinese]

[28] Z.X. Zhang, J.A. Sanchidrián, F. Ouchterlony, and S. Luukkanen, Reduction of fragment size from mining to mineral processing: a review, Rock Mech. Rock Eng., vol. 56, no. 1, pp. 747–778, 2023. DOI: 10.1007/s00603-022-03068-3.

[29] J.A. Sanchidrián, P. Segarra, F. Ouchterlony, and S. Gómez, The influential role of powder factor vs. delay in full-scale blasting: a perspective through the fragment size-energy fan, Rock Mech. Rock Eng., vol. 55, no. 7, pp. 4209–4236, 2022. DOI: 10.1007/s00603-022-02856-1.

[30] R.S. Yang, C.X. Ding, L.Y. Yang, Z. Lei, Z.R. Zhang, and Y.B. Wang, Visualizing the blast-induced stress wave and blasting gas action effects using digital image correlation, Int. J. Rock Mech. Min. Sci., vol. 112, pp. 47–54, 2018. DOI: 10.1016/j.ijrmms.2018.10.007.

[31] Z.X. Zhang, Rock Fracture and Blasting: Theory and Applications, Butterworth-Heinemann/Elsevier, Oxford, 2016.

[32] F. Ouchterlony, U. Myberg, M. Olsson, I. Bergqvist, L. Granlund, and H. Grind, Where does the explosive energy in rock blasting rounds go?, Sci. Technol. Energetic Mater., vol. 65, no. 2, pp. 54–63, 2004.

[33] J.A. Sanchidrián, P. Segarra, and L.M. López, Energy components in rock blasting, Int. J. Rock Mech. Min. Sci., vol. 44, no. 1, pp. 130–147, 2007. DOI: 10.1016/j.ijrmms.2006.05.002.

[34] W. Lu, Z. Leng, M. Chen, P. Yan, and Y. Hu, A modified model to calculate the size of the crushed zone around a blasthole, J. S. Afr. Inst. Min. Metall., vol. 116, no. 5, pp. 413–422, 2016. DOI: 10.17159/2411-9717/2016/v116n5a7.

[35] B. Rakishev, and Z.B. Rakisheva, Basic characteristics of the stages of rock massif destruction by explosive crushing, In: *Asia-Pacific Symposium on Blasting Techniques*, Kunming, China, 2011, pp. 65–69.

[36] H. Lin, J.T. Li, and P. Cao, Critical strain energy release rate test and its interrelated law of rock parameters, J. Central South Univ., vol. 44, no. 02, pp. 714–717, 2013. [in Chinese]